Journal of Earth Science, *Vol. 22*, *No. 2*, *p. 169–175*, *April 2011* *ISSN 1674-487X*
Printed in China
DOI: 10.1007/s12583-011-0169-6

Ab Initio Molecular Dynamic Simulation on the Elasticity of $Mg_3Al_2Si_3O_{12}$ Pyrope

Li Li*, **Donald J Weidner**
Mineral Physics Institute, *Department of Geosciences*, *University of New York at Stony Brook*, *Stony Brook*, *NY* 11790, *USA*
John Brodholt, **Dario Alfè**, **G David Price**
Department of Earth Sciences, *University College London*, *Gower Street*, *London WC*1*E*6*BT*, *UK*

ABSTRACT: We calculated thermo-elastic properties of pyrope ($Mg_3Al_2Si_3O_{12}$) at mantle pressures and temperatures using Ab initio molecular dynamic simulation. A third-order Birch-Murnaghan equation at a reference temperature of 2 000 K fits the calculations with bulk modulus, K_0=159.5 GPa, K_0'=4.3, V_0=785.89 Å^3, Grüneisen parameter, γ_0=1.15, q=0.80, Anderson Grüneisen parameter δ_T=3.76 and thermal expansion, $\alpha_0=2.93\times10^{-5}$ K^{-1}. Referenced to room temperature, where V_0=750.80 Å^3, γ_0 and α_0 become 1.11 and 2.47×10^{-5} K^{-1}. The elastic properties of pyrope are found to be nearly isotropic at transition zone conditions.

KEY WORDS: AIMD, thermo-elasticity, pyrope, high pressure.

INTRODUCTION

Silicate garnets are prominent minerals in the earth's mantle. They are stable over a wide depth range from the silicate garnets (pyrope $Mg_3Al_2Si_3O_{12}$, almandine $Fe_3Al_2Si_3O_{12}$, spessartine $Mn_3Al_2Si_3O_{12}$, grossular $Ca_3Al_2Si_3O_{12}$ and andradite $Ca_3Fe_2Si_3O_{12}$). Pyrope is considered to be the major end-member garnet in the earth's upper mantle and transition zone. The interpretation of seismic observations for the mantle relies on pressure-volume-temperature relations and both sound velocity values and anisotropies of constituent minerals at relevant pressure and temperature conditions. It is thus of primary importance to know the elasticity and thermal equation of state (EOS) of pyrope at mantle conditions when modelling seismic velocities and densities in the transition zone.

Elastic properties of pyrope have been the focus of extensive experimental and computational studies. Most of the high pressure experimental studies for pyrope were carried out at ambient temperature (Sinogeikin and Bass, 2000; Chen et al., 1999; Zhang and Herzberg, 1994) or high temperature-room pressure (Sinogeikin and Bass, 2002). Most recently, ultrasonic measurement was carried out up to 9 GPa and 1 000 ℃ (Gwanmesia et al., 2006). Current experimental data do not cover two important parameters: (1) pressure-temperature conditions relevant to the mantle; (2) anisotropies especially shear wave anisotropies which are crucial for interpreting seismic anisotropies (Deuss and Woodhouse, 2001). Computational studies have simulated thermodynamic properties and EOS of

This study was supported by the US NSF (No. EAR0809397), NERC (Nos. NER/T/S/2001/00855, NER/O/S/2001/01227), computer facilities provided by NERC at University College London, and the UK National Supercomputing Service (Hector).

*Corresponding author: lilli@ic.sunysb.edu

Manuscript received August 11, 2010.
Manuscript accepted November 12, 2010.

pyrope, but these studies used semi-empirical interatomic potentials (Mittal et al., 2001; Pavese, 1999). In recent years, Ab initio molecular dynamics (AIMD), which simulates stress-strain relationships at elevated pressure and temperature conditions, has been shown to be a more accurate method than semi-empirical approaches and may be used successfully to predict the structural and elastic properties of mantle silicates (Li et al., 2005; Stackhouse et al., 2004; Oganov et al., 2001a, b). In this article, we use the AIMD method to quantify thermo-elasticity of pyrope at mantle *P-T* conditions.

COMPUTATION METHOD

$Mg_3Al_2Si_3O_{12}$ pyrope has a cubic structure (Ia-3d space group); the tetrahedral (SiO_4) share corners with the octahedral (AlO_6). The atoms are in the following crystallographic sites: Mg(24c), Al(16a), Si(24d) and O(96h). For a body centred cubic (BCC) structure mineral like pyrope, its primitive cell has half the volume of a unit cell, and contains four formula units (80 atoms) in a parallelepiped unit cell. The primitive cell has three basis vectors of (1 -1 1), (1 1 -1) and (-1 1 1). All calculations were performed using this 80-atom primitive cell.

We used Vienna Ab-initio Simulation Package (VASP) code to perform our AIMD simulations (Kresse and Furthmüller, 1996a, b). We used projector-augmented-wave (PAW) implementation of density functional theory (DFT) (Blöchl, 1994) and the implementation of an efficient extrapolation for the charge density (Alfè, 1999). We used the exchange-correlation functional E_{xc} in the PW91 form of the generalized gradient approximation (GGA) (Perdew et al., 1992; Wang and Perdew, 1991). Γ point was used for sampling the Brillouin zone. The elastic constants were calculated at three volumes (774.2, 751.0 and 724.0 Å^3, volume term is used here rather than pressure because of the pressure correction term discussed below). At each volume, five temperatures are considered (0, 1 500, 2 000, 3 000 and 3 500 K). The plane-wave cut-off energy 500 eV is adequate as the effect of using a larger cut-off is found to be insignificant. At elevated temperatures, lattice parameters were fixed and the ionic positions were allowed to relax. The time step used in the dynamic simulation was 1 fs. The core radii were 2.0 a.u. for Mg (core configuration $1s^22s^2$), 1.9 a.u. for Al ($1s^22s^22p^6$), 1.5 a.u. for Si ($1s^22s^22p^6$) and 1.52 a.u. for O ($1s^2$). The equilibrium structure was obtained after at least 2 ps of simulation, when average stresses had converged to within 0.5 GPa. Applying strains (-1%, 1%, 2% and 2.5%) to the equilibrated structure, stresses were calculated over at least 1 ps of simulation. The linearity of stress vs. strain was carefully checked when elastic moduli were derived. The acoustic velocities as a function of crystallographic direction were derived from the calculated single-crystal elastic constants using Christoffel equation (Nye, 1957).

RESULTS AND DISCUSSION

Thermo-elasticity of Pyrope

The goal of this study is to calculate thermo-elastic properties of pyrope at mantle *P-T* conditions. We performed our calculations at five temperatures (0, 1 500, 2 000, 3 000 and 3 500 K) and three volumes (774.2, 751.0 and 724.0 Å^3). At first we define the elastic moduli, bulk modulus, shear modulus, and thermal pressure as a function of volume and temperature. From thermal pressure and bulk modulus, thermal expansion is defined.

Since we wish to define physical parameters along a geotherm, we define the reference state for equation of state as 2 000 K and 0 GPa. It is well known that generalized gradient approximation (GGA) model tends to overestimate the pressure when compared with experiment data (Oganov et al., 2001a), we have taken an approach to define, empirically, a pressure offset between the calculated pressure and measured pressure for a given volume (Li et al., 2009, 2006a, b, 2005; Oganov et al., 2001a). With the assumption that the calculations provide the correct physical property as a function of volume and temperature, we correct the pressure by combing our bulk modulus (K)-volume (V) relationship with the experimental volume adjusted to 2 000 K using the derived thermal expansion. We take V(298 K)=750.76 Å^3 (Leitner et al., 1980) and define V_0(2 000 K)=785.89 Å^3. We fitted our $K(V, T)$ results using a Birch Murnaghan equation of state and deduced K_0(2 000 K)=159.5 GPa, $(\partial K/\partial P)_T$=4.3, and $(\partial K/\partial T)_V$=0.003 3 GPa/K. With this equation of state, we calculated the

pressure at the investigated volumes, yielding a consistent 6.9(±0.1) GPa offset between the GGA pressure and the equation of state pressure, supporting our assumption of a constant pressure offset. Our previous studies have also shown that this offset is insensitive to both pressure and temperature as well (Li et al., 2005). In the following text, we use corrected pressure (P_c) to represent the pressure, P_c=P–6.9 GPa.

The 0 K calculations are compared with experimental data in Table 1. As can be seen, our results are in good agreement with previous reported calculations (Mittal et al., 2001; Pavese, 1999) and experimental results (Sinogeikin and Bass, 2000; Conrad et al., 1999; Leitner et al., 1980).

Table 1 Comparison of elastic moduli among this study and reported results

	P (GPa)	Density (g/cm^3)	c_{11} (GPa)	c_{12} (GPa)	c_{44} (GPa)	K (GPa)	G_{VRH} (GPa)	A	Method
This study	5.5	3.70	362	150	105	221	105	0.99	AIMD
This study	-1.5	3.57	312	118	94	183	95	0.97	AIMD
This study	-6.9	3.46	272	101	83	158	84	0.97	AIMD
Mittal et al., 2001	0	3.57	314	91	116	165	115	1.04	LD
Pavese, 1999	0	3.56	298	113	93	174	93	1.01	QH-LD
Conrad et al., 1999	0	3.58	298	110	93	172	93	0.99	BR
Leitner et al., 1980	0	3.56	295(2)	117(1)	90(3)	177(1)	89(1)	1.01	BR
Sinogeikin and Bass, 2000	0	3.56	297	108	93	171	94	0.98	BR
Sinogeikin and Bass, 2000	14	3.81	372	153	111	226	110	1.01	BR

AIMD. Ab initio molecular dynamics; LD. shell-model lattice dynamics calculation; QH-LD. quasi-harmonic approximation lattice dynamics simulation using empirical potentials; BR. Brillouin scattering. The calculated results are at 0 K; the experimental results are at room temperature. c_{11}, c_{12} and c_{44} are the single crystal moduli; K is the bulk modulus; G_{VRH} is the Voigt-Reuss-Hill average of shear modulus; A is the anisotropy, $A=2c_{44}/(c_{11}-c_{12})$. The three listed pressures for this study are the corrected pressure P_c=P–6.9 GPa.

Table 2 Calculated elastic constants for pyrope at high pressure and high temperature

P_c (GPa)	T (K)	Density (g/cm^3)	c_{11} (GPa)	c_{12} (GPa)	c_{44} (GPa)	K (GPa)	G_{VRH} (GPa)	A	V_p (km/s)	V_s (km/s)
13.0(3)	1 500	3.70	355	165	102	229	99	1.07	9.87	5.17
5.7(4)	1 500	3.57	309	126	92	187	92	1.00	9.32	5.07
0.6(3)	1 500	3.46	286	118	88	176	86	1.05	9.14	4.99
15.5(4)	2 000	3.70	340	155	97	217	95	1.05	9.64	5.08
8.2(4)	2 000	3.57	316	142	93	200	91	1.07	9.49	5.05
3.1(5)	2 000	3.46	266	119	76	168	75	1.03	8.79	4.65
20.1(4)	3 000	3.70	332	162	89	219	87	1.04	9.52	4.86
13.1(4)	3 000	3.57	308	136	84	193	85	0.98	9.27	4.88
7.6(4)	3 000	3.46	273	127	79	176	76	1.08	8.96	4.70
22.6(4)	3 500	3.70	358	169	100	232	97	1.06	9.89	5.13
15.1(4)	3 500	3.57	324	154	85	211	85	1.00	9.54	4.89
10.1(5)	3 500	3.46	275	116	78	169	78	0.98	8.90	4.76

Error analysis for the pressures was performed by reblocking the data, as described elsewhere (Allen and Tildesley, 1997). The errors of single crystal elastic moduli are about 5%. P_c is the corrected pressure P_c=P–6.9 GPa.

Table 3 Thermal expansion (α), Grüneisen parameter (γ), thermal pressure (P_{th}) at high pressure and temperature (T)

V (Å^3)	T (K)	P_c (GPa)	P_{th} (GPa)	$(\partial P/\partial T)_V$ (GPa· K^{-1})	α (K^{-1})	γ
724.0	1 500	13.0	7.4	4.86×10^{-3}	2.17×10^{-5}	1.09
	2 000	15.5	9.9			1.09
	3 000	20.1	14.5			1.07
	3 500	22.6	17.0			1.07
751.0	1 500	5.7	7.2	4.79×10^{-3}	2.42×10^{-5}	1.10
	2 000	8.2	9.7			1.11
	3 000	13.1	14.6			1.12
	3 500	15.1	16.5			1.08
774.2	1 500	0.6	7.3	4.82×10^{-3}	2.80×10^{-5}	1.15
	2 000	3.1	9.8			1.16
	3 000	7.6	14.3			1.13
	3 500	10.1	16.8			1.14

P_c is the corrected pressure, P_c=P–6.9 GPa.

The calculated single crystal elastic moduli are listed in Table 2. We fit the aggregate shear modulus with a third order Eulerian strain equation of state (Bina and Helffrich, 1992) given by $G=G_0(1+2f)^{5/2}\{1-f[5-3(\partial G^0/\partial P)_T(K_0/G^0)]\}+(\partial G/\partial T)_V$, where $f=\frac{1}{2}[(V_0/V)^{2/3}-1]$. Referenced to 2 000 K, we find G_0= 79.05 GPa, $(\partial G/\partial P)_T$=2.68, and $(\partial G/\partial T)_V$=-0.002 1 GPa/K indicating anharmonic contributions to the shear modulus. The anisotropy $A=2c_{44}/(c_{11}-c_{12})$ remains close to 1 (between 0.98 and 1.08) at all pressures and temperatures considered.

The thermal parameters are calculated and listed in Table 3. Thermal expansion α is obtained from $(\partial P/\partial T)_V/K_T$. Since the bulk modulus K_T is relatively insensitive to temperature at constant volume within the error of calculated pressure, the thermal expansion also becomes temperature insensitive at constant volume in the calculated P-T conditions. The Grüneisen parameter, $\gamma(V)$, is calculated from the thermal pressure and thermal energy: $\gamma(V)=P_{th}(V, T)V/E_{th}(V, T)$, where the thermal energy $E_{th}=3(N-1)k_bT$, with k_b is the Boltzmann constant; N is the number of atoms in the supercell (N=80 in this study). As we can see in Table 3, the dependence of $\gamma(V)$ on temperature is insignificant. Using V_0(298 K)=750.76 Å^3 (Leitner et al., 1980) to fit the relation: $\gamma=\gamma_0(V/V_0)^q$, we obtain γ_0=1.11 and q=0.80±0.05 at room temperature. The Anderson Grüneisen parameter, δ_T, is given by

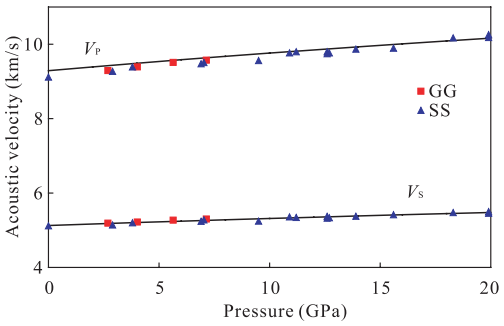

Figure 1. Pyrope sound velocities at room pressure. Solid lines are those calculated using the Ab initio molecular dynamics, square symbols (GG) are experimental ultrasonic data reported by Gwanmesia et al. (2006), triangles (SS) are from Brillouin spectroscopy reported by Sinogeikin and Bass (2000).

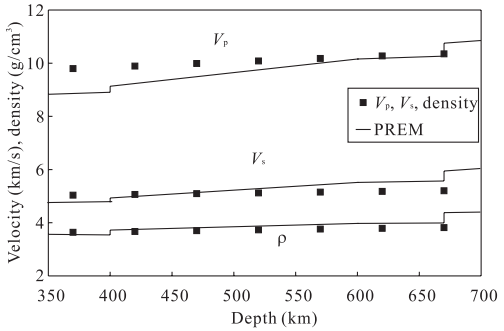

Figure 2. Density (ρ) and sound velocities (V_p, V_s) of pyrope derived along the geotherm (Brown and Shankland, 1981); plotted as symbols. Also plotted (solid lines) are the PREM values.

$\delta_T=(\partial \ln\alpha/\partial \ln V)_T$. Our best fit values are δ_T=3.76±0.05 and α_0=2.47×10^{-5} K^{-1} referred 298 K.

The derived equation of state parameters (referenced to 2 000 K) are given in Table 4. Our calculations are mostly at high temperature (above the Debye temperature of pyrope, 790 K (Wang et al., 1998)) and since the earth's mantle is also at high temperature, we define the reference condition for the equation of state as zero pressure and 2 000 K.

Table 4 Pressure-volume equation of state parameters for zero pressure and 2 000 K

Property	Value
V (Å^3)	785.89(5)
α (10^{-5}K^{-1})	2.93
δ	3.76(5)
γ	1.15
q	0.8
K_T^0 (GPa)	159.5(6)
$(\partial K_T/\partial P)_T$	4.3(2)
$(\partial K_T/\partial T)_V$ (GPa/K)	0.003 3
G^0 (GPa)	79.05
$(\partial G/\partial P)_T$	2.68
$(\partial G/\partial T)_V$ (GPa/K)	-0.002 8

A third order Birch-Murnaghan fitting of the AIMD bulk modulus vs. volume and corrected-pressure vs. volume yield these 2 000 K reference state variables.

With these values, we derive the expected longitudinal and shear velocities as a function of pressure and at room temperature for comparison with existing data. Figure 1 compares our calculations (solid lines) with the room-temperature data of Gwanmesia et al. (2006) and Sinogeikin and Bass (2002, 2000) as indicated by the symbols. They reported measured acoustic velocities at pressures up to 20 GPa. As can be seen in this figure, our equation of state, based on AIMD calculations and the zero pressure volume, fits the observations extremely well. This gives us confidence that these calculations should equally well predict the acoustic velocities at the conditions of the transition zone, the region of P-T space that was spanned for the calculations.

GEOPHYSICAL IMPLICATION

Our understanding of the structure of the mantle is constrained by seismic observations which need to be coupled the properties of the mantle minerals for interpretation (Li and Weidner, 2008). The knowledge of shear wave properties is crucial since consistent evidence of some weak discontinuities such as 520 km come from SS precursors (Deuss and Woodhouse, 2001; Gu et al., 1998; Gossler and Kind, 1996; Shearer, 1990) or ScS reverberations (Revenaugh and Jordan, 1991). The information about shear wave properties from our results underscores the importance of AIMD calculation.

Table 5 Computed maximum and minimum P-and S-ware velocities at T=0 K (for V=774.2 Å^3); and T=2 000 K (for V=724.0, 751.0 and 774.2 Å^3)

Volume	724.0 Å^3	751. 0 Å^3	774.2 Å^3	774.2 Å^3
Temperature (K)	2 000	2 000	2 000	0
Pressure (GPa)	15.5	8.2	3.1	-6.9
V_{Pmax} (km·s^{-1})	9.67	9.53	8.82	8.87
V_{Pmin} (km·s^{-1})	9.59	9.41	8.60	8.81
V_{Pmax}/V_{Pmin}	1.01	1.00	1.02	1.01
V_{Smax} (km·s^{-1})	5.12	5.10	4.69	4.97
V_{Smin} (km·s^{-1})	5.00	4.94	4.53	4.90
V_{Smax}/V_{Smin}	1.02	1.03	1.03	1.01
$(V_{SH}/V_{SV})_{max}$	1.02	1.03	1.03	1.01

The maximum P wave direction is (111); the minimum P wave direction is (001); the maximum S wave direction is (110); the minimum S wave direction is (001) as dictated by the cubic symmetry.

With the thermo-elasticity results listed above, one can derived the density and velocities of pyrope at mantle pressure and temperature. The adiabatic bulk modulus (K_s) was obtained from the calculated isothermal bulk modulus (K_T) by $K_s=K_T(1+\alpha\gamma T)$. The results are shown in Fig. 2. We can see that the two velocities and density of pyrope increase with depth, but with a smaller slope compared with PREM (preliminary reference earth model). Above the 410 discontinuity, the velocities and density of pyrope are higher than those of PREM, with the P-wave velocity being 8% higher than PREM at 400 km. At the 660 discontinuity the P-wave velocity is equal to the PREM value while the shear velocity is 14% lower than that of PREM. A detailed comparison of the absolute values of velocities and density still awaits further study on the effects of composition on the elastic properties and density of garnet.

Our results predict that elastic properties of pyrope remain nearly isotropic in the transition zone. Table 5 lists the calculated sound velocities at 2 000 K for three volumes (V=724.0, 751.0 and 774.2 Å^3) and at 0 K for one volume (V=774.2 Å^3). The P wave and S wave are nearly isotropic for the four conditions. A global seismic study (Montagner and Kennett, 1996) reported a 2%–4% anisotropy in the lower part of the transition zone while another study reported a upper bound of 0.5% S-wave anisotropy below the Tonga subduction zone (Fisher and Wiens, 1996). Seismic anisotropy may be a result of presence of akimotoite (Li et al., 2009) or texture due to plastic flow. Our results indicate that pyrope does not contribute the anisotropy in the transition zone. Again, the effect of composition still awaits further study.

REFERENCES CITED

Alfè, D., 1999. Ab Initio Molecular Dynamics, a Simple Algorithm for Charge Extrapolation. *Computer Physics Communications*, 118(1): 31–33

Allen, M. P., Tildesley, D. J., 1997. Computer Simulation of Liquids. Oxford University Press, New York. 408

Bina, C. R., Helffrich, G. R., 1992. Calculation of Elastic Properties from Thermodynamic Equation of State Principles. *Annu. Rev. Earth Planet. Sci.*, 20: 527–552

Blöchl, P. E., 1994. Projector Augmented-Wave Method. *Phys. Rev. B*, 50(24): 17953–17979

Brown, J. M., Shankland, T. J., 1981. Thermodynamic Parameters in the Earth as Determined from Seismic Profiles. *Geophys. J. R. Astr. Soc.*, 66(3): 579–596

Chen, G. L., Cooke, J. A., Gwanmesia, G. D., et al., 1999. Elastic Wave Velocities at $Mg_3Al_2Si_3O_{13}$—Pyrope Garnet to 10 GPa. *American Mineralogist*, 84(3): 384–388

Conrad, P. G., Zha, C. S., Mao, H. K., et al., 1999. The High-Pressure, Single-Crystal Elasticity of Pyrope, Grossular, and Andradite. *American Mineralogist*, 84(3): 374–383

Deuss, A., Woodhouse, J., 2001. Seismic Observations of Splitting of the Mid-transition Zone Discontinuity in Earth's Mantle. *Science*, 294(5541): 354–357

Fisher, K. M., Wiens, D. A., 1996. The Depth Distribution of Mantle Anisotropy beneath the Tonga Subduction Zone. *Earth and Planetary Science Letters*, 142(1–2): 253–260

Gossler, J., Kind, R., 1996. Seismic Evidence for very Deep Roots of Continents. *Earth and Planetary Science Letters*, 138(1–4): 1–13

Gu, Y., Dziewonski, A. M., Agee, C. B., 1998. Global De-correlation of the Topography of Transition Zone Discontinuities. *Earth and Planetary Science Letters*, 157(1–2): 57–67

Gwanmesia, G. D., Zhang, J., Darling, K., et al., 2006. Elasticity of Polycrystalline Pyrope ($Mg_3Al_2Si_3O_{12}$) to 9 GPa and 1 000 ℃. *Physics of the Earth and Planetary Interiors*, 155(3–4): 179–190

Kresse, G., Furthmüller, J., 1996a. Efficiency of Ab-Initio Total Energy Calculations for Metals and Semiconductors Using a Plane-Wave Basis Set. *Comput. Mat. Sci.*, 6(1): 15–50

Kresse, G., Furthmüller, J., 1996b. Efficient Iterative Schemes for Ab Initio Total-Energy Calculations Using a Plane-Wave Basis Set. *Phys. Rev. B*, 54(16): 11169–11186

Leitner, B. J., Weidner, D. J., Liebermann, R. C., 1980. Elasticity of Single Crystal Pyrope and Implications for Garnet Solid Solution Series. *Physics of the Earth and Planetary Interiors*, 22(2): 111–121

Li, L., Weidner, D. J., 2008. Effect of Phase Transitions on Bulk Dispersion and Attenuation: Implications for the Earth. *Nature*, 454: 984–986

Li, L., Weidner, D. J., Brodholt, J., et al., 2005. Phase Stability of $CaSiO_3$ Perovskite at High Pressure and Temperature: Insights from Ab Initio Molecular Dynamics. *Physics of the Earth and Planetary Interiors*, 155(3–4): 260–268

Li, L., Weidner, D. J., Brodholt, J., et al., 2006a. Elasticity of Mg_2SiO_4 Ringwoodite at Mantle Conditions. *Physics of*

the Earth and Planetary Interiors, 157(3–4): 181–187

Li, L., Weidner, D. J., Brodholt, J., et al., 2006b. Elasticity of $CaSiO_3$ Perovskite at High Pressure and High Temperature. *Physics of the Earth and Planetary Interiors*, 155(3–4): 249–259

Li, L., Weidner, D. J., Brodholt, J., et al., 2009. Ab Initio Molecular Dynamics Study of Elasticity of Akimotoite $MgSiO_3$ at Mantle Conditions. *Physics of the Earth and Planetary Interiors*, 173(1–2): 115–120

Mittal, R., Chaplot, S. L., Choudhury, N., 2001. Lattice Dynamics Calculations of the Phonon Spectra and Thermodynamic Properties of the Aluminosilicate Garnets Pyrope, Grossular, and Spessartine $M_3Al_2Si_3O_{12}$ (M=Mg, Ca, and Mn). *Phys. Rev. B*, 64(9): 094302

Montagner, J. P., Kennett, B. L. N., 1996. How to Reconcile Body-Wave and Normal Mode—Reference Earth Models. *Geophys. J. Int.*, 125(1): 229–248

Nye, J. F., 1957. Physical Properties of Crystals. Oxford University Press, Ely House, London

Oganov, A. R., Brodholt, J. P., Price, G. D., 2001a. Ab Initio Elasticity and Thermal Equation of State of $MgSiO_3$ Perovskite. *Earth and Planetary Science Letters*, 184(3–4): 555–560

Oganov, A. R., Brodholt, J. P., Price, G. D., 2001b. The Elastic Constants of $MgSiO_3$ Perovskite at Pressures and Temperatures of the Earth's Mantle. *Nature*, 411(6840): 934–937

Pavese, A., 1999. Quasi-harmonic Computer Simulations of the Structural Behaviour and EOS of Pyrope at High Pressure and High Temperature. *Phys. Chem. Minerals*, 26(8): 649–657

Perdew, J. P., Chevary, J. A., Vosko, S. H., et al., 1992. Atoms, Molecules, Solids, and Surfaces: Applications of the Generalized Gradient Approximation for Exchange and Correlation. *Phys. Rev. B*, 46(11): 6671–6687

Revenaugh, J., Jordan, T. H., 1991. The ScS Phase in the Reflection of S-Waves from the Core-Mantle Boundary. *Journal of Geophysical Research-Solid Earth*, 96(B12): 19763−19780

Shearer, P. M., 1990. Seismic Imaging of Upper-Mantle Structure with New Evidence for a 520-km Discontinuity. *Nature*, 344(6262): 121–126

Sinogeikin, S. V., Bass, J. D., 2000. Single-Crystal Elasticity of Pyrope and MgO to 20 GPa by Brillouin Scattering in the Diamond Cell. *Physics of the Earth and Planetary Interiors*, 120(1–2): 43–62

Sinogeikin, S. V., Bass, J. D., 2002. Elasticity of Pyrope and Majorite-Pyrope Solid Solutions to High Temperatures. *Earth and Planetary Science Letters*, 203(1): 549–555

Stackhouse, S., Brodholt, J. P., Wookey, J., et al., 2004. The Effect of Temperature on the Seismic Anisotropy of the Perovskite and Post-Perovskite Polymorphs of $MgSiO_3$. *Earth and Planetary Science Letters*, 230(1–2): 1–10

Wang, Y., Perdew, J. P., 1991. Correlation Hole of the Spin-Polarized Electron-Gas, with Exact Small-Wave-Vector and High Density Scaling. *Phy. Rev. B*, 44(24): 13298–13307

Wang, Y., Weidner, D. J., Zhang, J. Z., et al., 1998. Thermal Equation of State of Garnets along the Pyrope-Majorite Join. *Physics of the Earth and Planetary Interiors*, 105(1–2): 59–71

Zhang, J., Herzberg, C., 1994. Melting of Pyrope, $Mg_3Al_2Si_3O_{12}$, at 7–16 GPa. *American Mineralogist*, 79(5–6): 497–503